Signatures of the Many Supermassive Black Hole Mergers in a Cosmologically Forming Massive Early-type Galaxy

Mannerkoski, Matias

2022-04-26

Mannerkoski , M , Johansson , P H , Rantala , A , Naab , T , Liao , S & Rawlings , A 2022 , ' Signatures of the Many Supermassive Black Hole Mergers in a Cosmologically Forming Massive Early-type Galaxy ' , Astrophysical Journal , vol. 929 , no. 2 , 167 . https://doi.org/10.3847/1538-4357/ac5f0b

http://hdl.handle.net/10138/343080
https://doi.org/10.3847/1538-4357/ac5f0b

The Astrophysical Journal, 929:167 (9pp), 2022 April 20 https://doi.org/10.3847/1538-4357/ac5f0b

Signatures of the Many Supermassive Black Hole Mergers in a Cosmologically Forming Massive Early-type Galaxy

Matias Mannerkoski[1], Peter H. Johansson[1], Antti Rantala[2], Thorsten Naab[2], Shihong Liao[1], and Alexander Rawlings[1]
[1] Department of Physics, Gustaf Hällströmin katu 2, FI-00014, University of Helsinki, Finland; matias.mannerkoski@helsinki.fi
[2] Max-Planck-Institut für Astrophysik, Karl-Schwarzchild-Str 1, D-85748 Garching, Germany
Received 2021 December 2; revised 2022 February 28; accepted 2022 March 16; published 2022 April 26

Abstract

We model here the merger histories of the supermassive black hole (SMBH) population in the late stages of a cosmological simulation of a $\sim 2 \times 10^{13} M_{\odot}$ galaxy group. The gravitational dynamics around the several tens of SMBHs ($M_\bullet > 7.5 \times 10^7 M_{\odot}$) hosted by the galaxies in the group is computed at high accuracy using regularized integration with the KETJU code. The 11 SMBHs that form binaries and a hierarchical triplet eventually merge after hardening through dynamical friction, stellar scattering, and gravitational wave (GW) emission. The binaries form at eccentricities of $e \sim 0.3$–0.9, with one system evolving to a very high eccentricity of $e = 0.998$, and merge on timescales of a few tens to several hundred megayears. During the simulation, the merger-induced GW recoil kicks eject one SMBH remnant from the central host galaxy. This temporarily drives the galaxy off the $M_\bullet$–$\sigma_\star$ relation; however, the galaxy returns to the relation due to subsequent galaxy mergers, which bring in new SMBHs. This showcases a possible mechanism contributing to the observed scatter of the $M_\bullet$–$\sigma_\star$ relation. Finally, we show that pulsar timing arrays and *LISA* would be able to detect parts of the GW signals from the SMBH mergers that occur during the ∼4 Gyr time span simulated with KETJU.

Unified Astronomy Thesaurus concepts: Supermassive black holes (1663); Galaxy mergers (608); Astronomical simulations (1857); Gravitational wave sources (677)

1. Introduction

The masses of the central supermassive black holes (SMBHs) in massive galaxies are tightly correlated with the structural properties of their host galaxies, which is manifested in the observed $M_\bullet$–$\sigma_\star$ relation (e.g., Kormendy & Ho 2013). Massive early-type galaxies are believed to have assembled through a two-stage process, in which the early assembly is dominated by rapid in situ star formation in gas-rich systems, whereas the later growth below redshifts of $z \lesssim 2$–3 is dominated by relatively gas-poor minor mergers (e.g., Johansson et al. 2012; Naab & Ostriker 2017). During galaxy mergers, SMBHs merge through a three-stage process (Begelman et al. 1980), driven first by dynamical friction until a binary forms, then by three-body scattering between the SMBH binary and individual stars (Hills & Fullerton 1980), and finally at subparsec scales by gravitational wave (GW) emission (Peters 1964).

The GW emission from a binary is in general asymmetric due to the different SMBH masses and spins. This produces a recoil kick, typically giving the merged SMBH a velocity $\lesssim 500\ \mathrm{km\ s^{-1}}$, but reaching $\sim 4000\ \mathrm{km\ s^{-1}}$ for suitable spins (e.g., Campanelli et al. 2007). Large kick velocities can significantly displace the merged SMBH or even eject it from the galaxy. This has been suggested to give rise to the observed offset active galactic nuclei (e.g., Comerford et al. 2015), drive the formation of large galactic cores (Nasim et al. 2021), and contribute to the scatter in the $M_\bullet$–$\sigma_\star$ relation (Volonteri 2007; Blecha et al. 2011).

The GWs emitted during the final phases of an SMBH merger could be detectable by ongoing pulsar timing array (PTA) projects, which primarily target the stochastic superposition of GWs from the expected large number of SMBH binaries (e.g., Arzoumanian et al. 2020) but may also detect individual loud sources. The PTAs are most sensitive to GWs in the nanohertz frequency range and therefore target very massive SMBHs $M_\bullet \gtrsim 10^8 M_{\odot}$, with orbital periods of around a few years (e.g., Kelley et al. 2017). The *Laser Interferometer Space Antenna* (*LISA*) (Amaro-Seoane et al. 2017) is a planned space-based detector that will mainly target the GWs emitted during the inspiral and merger of slightly lower-mass SMBHs of $M_\bullet \sim 10^6$–$10^7 M_{\odot}$ up to very high redshifts. However, the final parts of the signals from low-redshift mergers of SMBH binaries with masses around $M_\bullet \sim 10^8 M_{\odot}$ are also expected to be detectable with *LISA* (Katz & Larson 2019).

The small-scale dynamics of SMBHs in merging galaxies have been studied extensively in isolated collisionless galaxy mergers (e.g., Berentzen et al. 2009; Khan et al. 2011; Rantala et al. 2018; Nasim et al. 2021); however, to date only very few high-resolution cosmological zoom-in simulations with detailed SMBH dynamics have been carried out (Khan et al. 2016a; Mannerkoski et al. 2021). Instead, studies of merging SMBH binaries in a cosmological context have typically made use of semi-analytic methods (e.g., Kelley et al. 2017; Bonetti et al. 2019; Izquierdo-Villalba et al. 2022), which make several assumptions about the unresolved binary orbits, some of which may not be fully motivated.

In this paper we study the dynamics of SMBHs and their GW signals in a cosmological zoom-in simulation of a group-sized halo hosting dozens of SMBHs with masses $M_\bullet \gtrsim 10^8 M_{\odot}$. The simulation is run using our updated KETJU code (Rantala et al. 2017, 2018; Mannerkoski et al. 2021), which is able to resolve the dynamics of merging SMBH down to tens of Schwarzschild radii. We now also include a model for GW

recoil kicks, which allows us to study the displacement and ejection of SMBHs from their host galaxies.

This paper is structured as follows. In Section 2 we give a brief overview of the KETJU code and describe our simulation setup. In Section 3 we first describe the general properties of the simulated SMBH mergers, highlighting also the structural and kinematic properties of their host galaxies. This is followed by a discussion of the evolution of the SMBHs on the $M_\bullet$–$\sigma_\star$ plane. We round off this section with a calculation of the detectability of our simulated GW signals. In Section 4 the validity and implications of our results are discussed, and finally, in Section 5, we present our conclusions.

2. Numerical Simulations

2.1. The KETJU Code

The KETJU code extends the widely used GADGET-3 code (Springel 2005) by replacing the standard leapfrog integration of SMBHs and their surrounding stellar particles with the high-accuracy regularized MSTAR integrator (Rantala et al. 2020) in a small region around each SMBH. All SMBH–SMBH and SMBH–stellar particle interactions in the regularized regions are computed without gravitational softening, while the gravitational interactions between stellar particles are softened to avoid energy errors when particles enter and exit the regions. The center-of-mass motion of the regularized regions is integrated using the same leapfrog integrator that is used for all the other particles, and the small perturbing tidal forces acting on the regions are also included through leapfrog kicks instead of the computationally more costly but also slightly more accurate perturber particle method used in earlier KETJU versions (Rantala et al. 2017, 2018).

Post-Newtonian (PN) corrections are included in interactions between SMBHs to account for relativistic effects such as GW emission. In addition to binary PN terms, we now also include the leading order 1PN corrections of a general N-body system, which contain terms involving up to three bodies that may affect the long-term evolution of triplet SMBH systems (Will 2014; Lim & Rodriguez 2020). This is done using the expressions from Thorne & Hartle (1985) for the 1PN and spin terms, whereas higher-order corrections valid for BH binary systems up to 3.5PN order are adopted from Equation (203) of Blanchet (2014).

In addition, we now include a model for the mass, spin, and recoil velocity of SMBH merger remnants based on the numerical relativity fitting functions from Zlochower & Lousto (2015). The model uses as inputs the spins and orbital orientation of the BH binary when it is merged at a separation of $12G(M_1+M_2)/c^2$, where $M_{1,2}$ are the component masses. This gives remnant properties that account for the particular spin directions and orbital orientation of the SMBHs determined by their prior evolution, but which are still only approximate due to the inherent limitations of the fit functions.

We use the same hydrodynamics, star formation, and feedback models as in Mannerkoski et al. (2021). The hydrodynamics of gas is modeled using the SPHGal smoothed particle hydrodynamics (SPH) implementation (Hu et al. 2014), which employs a pressure-entropy formulation together with artificial conduction and viscosity utilizing a Wendland C^4-kernel smoothed over 100 neighbors. Our models include metal-dependent cooling that tracks 11 individual elements and stochastic star formation with a critical hydrogen number density threshold of $n_{\rm H}=0.1\,{\rm cm}^{-3}$ (Scannapieco et al. 2005, 2006; Aumer et al. 2013). In addition we include models for feedback from supernovae and massive stars, as well as the production of metals through stellar chemical evolution (Aumer et al. 2013; Eisenreich et al. 2017).

Galaxies with dark matter (DM) halo masses of $M_{\rm DM}=10^{10}h^{-1}M_\odot$ are seeded with black holes with masses of $M_\bullet=10^5h^{-1}M_\odot$, which then grow through gas accretion and merging (Sijacki et al. 2007). The accretion onto SMBHs is modeled using a simple Bondi–Hoyle–Lyttleton prescription with an additional dimensionless multiplier of $\alpha=25$ to account for the limited spatial resolution (Johansson et al. 2009b). The maximum accretion rate is capped at the Eddington limit, and, assuming a fixed radiative efficiency of $\epsilon_r=0.1$, a total of 0.5% of the rest mass energy of the accreted gas is coupled to the surrounding gas as thermal energy (Springel et al. 2005). This model successfully produces SMBHs in agreement with the observed scaling relations, but does not correctly model the accretion onto tight binaries or the evolution of SMBH spin. However, these shortcomings are not significant, as the SMBH binaries in this study are predominantly found in gas-poor environments and thus have low gas accretion rates.

2.2. Initial Conditions and Simulations

We run a cosmological zoom-in simulation starting at a redshift of $z=50$, targeting a much larger volume than in Mannerkoski et al. (2021). The high-resolution region is centered on a DM halo with a virial mass of $M_{200}\sim 2.5\times10^{13}M_\odot$, covering an initial comoving size of $(10h^{-1}\,{\rm Mpc})^3$ and containing 410^3 of both gas and DM particles with masses of $m_{\rm gas}=3\times10^5M_\odot$ and $m_{\rm DM}=1.6\times10^6M_\odot$. The initial conditions are generated with the MUSIC (Hahn & Abel 2011) software package using the Planck 2018 cosmology (Planck Collaboration et al. 2020) with a Hubble parameter of $h=0.674$.

We first evolve this volume with standard GADGET-3 including SMBH seeding and repositioning until $z=0.815$, at which point the simulation contains tens of galaxies hosting SMBHs with masses $>7.5\times10^7M_\odot$. We take this as the lower mass limit of SMBHs to be modeled with KETJU, because a high enough SMBH to stellar particle mass ratio is required to ensure accurate binary dynamics (Mannerkoski et al. 2021). For this initial run, the gravitational softening lengths were set to $\epsilon_{\rm bar}=40h^{-1}$ pc for stars and gas, and $\epsilon_{\rm DM,high}=93h^{-1}$ pc for high-resolution dark matter particles.

We continue the run from $z=0.815$ with KETJU. For this run, we lower the softening length of the stellar particles to $\epsilon_\star=20h^{-1}$ pc to allow using regularized regions with radii of $60h^{-1}$ pc, resulting in a manageable level of a few thousand stellar particles in each regularized region.

At this point we also add spins to the SMBH particles to model their merger recoil kicks. The spin directions are generated from a uniform distribution on the sphere, whereas the spin magnitudes use the distribution from Lousto et al. (2010), resulting in dimensionless spins $\chi=cJ/GM^2\sim0.5$–0.9, where J is the spin angular momentum. Observations constrain the spins of SMBHs with masses above $10^8M_\odot$ rather poorly, but are consistent with their spins being in this range (Reynolds 2019). During the simulation, the dimensionless spin may decrease slightly as the gas accretion

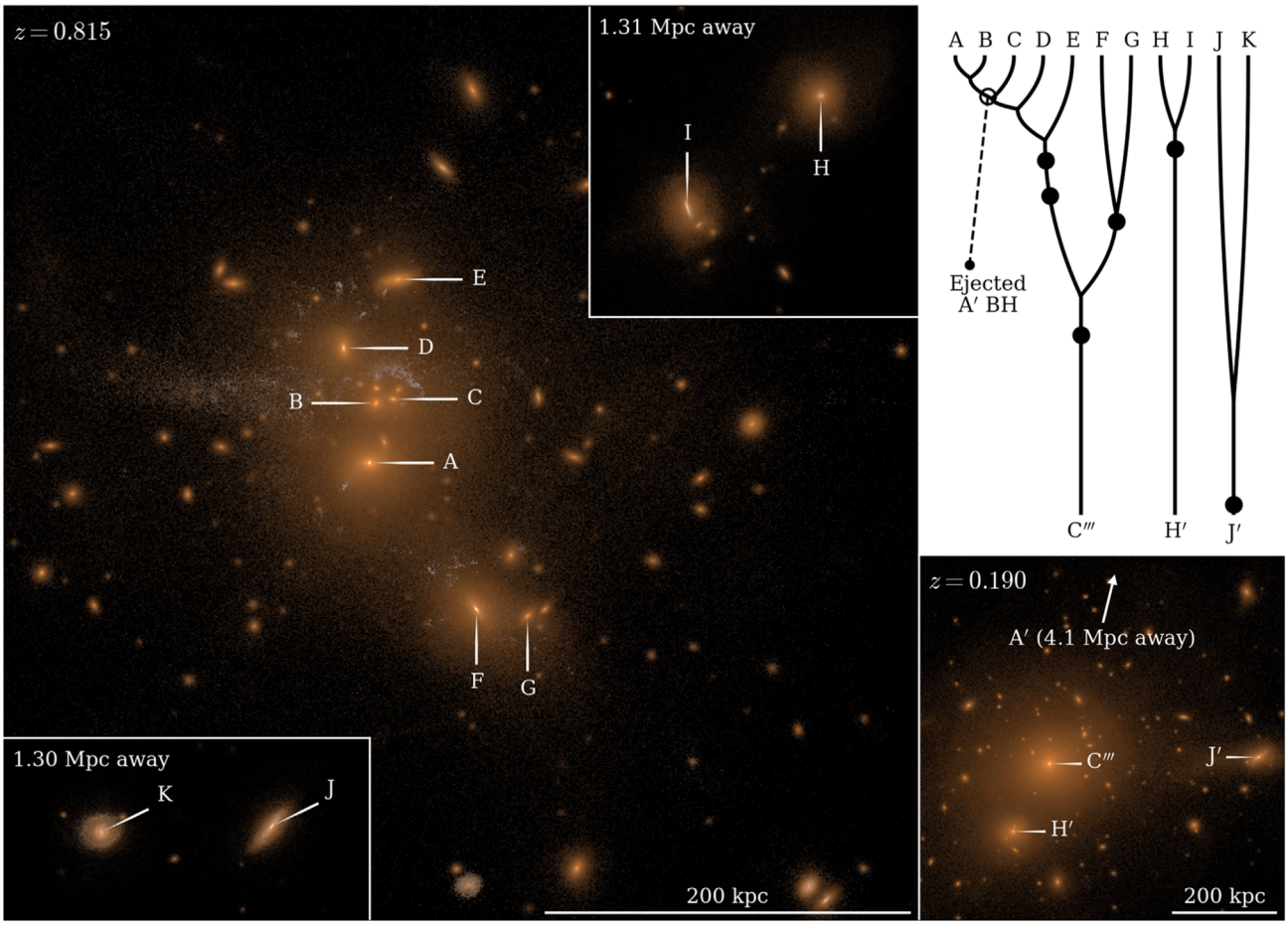

Figure 1. *Left:* The galaxies and SMBHs of interest in the initial state of the KETJU run. The main panel shows the central group of galaxies, with the two more distant pairs of galaxies shown in the corners at the same spatial scale. The images are generated from BVR-luminosities accounting only for stellar emission. *Top right:* A schematic merger tree of the galaxies and SMBHs with time progressing from top to bottom. The lines follow the galaxy mergers, while the circles indicate SMBH binary mergers. *Bottom right:* The final state of the simulation with the remaining SMBHs labeled.

model does not yet evolve the spin angular momentum, while the mass of the SMBHs may increase.

3. Results

3.1. Galaxy and SMBH Mergers

At the start of the KETJU simulation there are a total of 11 galaxies hosting massive SMBHs that are involved in mergers over the course of the simulation. These galaxies are shown in the left panel of Figure 1, with the labels marking the locations of the SMBHs (e.g., A), with the host galaxies being referred to as, e.g., gA.

Seven of the galaxies (gA–gG) are in a central group that is collapsing within a halo with a total virial mass of $M_{200} \approx 2 \times 10^{13} M_\odot$ and a virial radius of $R_{200} \approx 420$ kpc. In addition, there are two pairs of galaxies (gH and gI, gK, and gJ) on their initial orbits before merging. They are within halos of $M_{200} \approx 2.5 \times 10^{12} M_\odot$, $R_{200} \approx 220$ kpc for the gH–gI pair and $M_{200} \approx 1.3 \times 10^{12} M_\odot$, $R_{200} \approx 170$ kpc for the gJ–gK pair. The properties of these galaxies and their SMBHs are listed in Table 1. Finally, there are another 19 galaxies in the simulation volume, which host SMBHs that are to begin with or later grow to be massive enough to be modeled with KETJU, as well as a large number of lower-mass SMBHs. However, they do not interact with the more massive SMBHs studied here.

In Figure 2 we show the density, velocity, and axis ratio profiles of three selected galaxies (gA, gH, and gJ). The galaxies are clearly triaxial at the start of the KETJU run, and show moderately fast rotation with $V/\sigma_\star \sim 0.5$ in their outer parts. The density profiles are flattened in the centers, resulting in galactic cores with radii of a few hundred parsec, which are caused by the impact of gravitational softening. However, in general the structural and kinematic properties of our simulated galaxies are in good agreement with the observed properties of $z = 0.8$ galaxies (e.g., Bezanson et al. 2018), although the half-mass radii of our simulated galaxies are toward the lower end of the observed range.

As the simulation progresses, the galaxies merge in the order shown in the top right panel of Figure 1. The final state of the simulation at $z = 0.19$ is shown in the lower right panel of Figure 1. The simulation is stopped at this point as there are no more imminent galaxy mergers involving massive SMBHs. The properties of the galaxies in this final output are also listed in Table 1, and their density, velocity, and shape profiles are included in Figure 2. The galaxies evolve as expected, with the sizes and velocity dispersions increasing, while the rotational velocities and triaxialities mainly decrease. The central flattening of the density profile is also somewhat reduced because the SMBHs are resolved as non-softened point masses.

The galaxy mergers result in bound SMBH binaries that harden and finally merge due to stellar interactions and GW

Table 1
Properties of the SMBHs and Their Host Galaxies

BH Label[a]	$M_\bullet/10^8 M_\odot$[b]	$M_\bullet/m_\star$[c]	χ[d]	$v_{\rm kick}/{\rm km\ s^{-1}}$[e]	$M_\star/10^{10} M_\odot$[f]	$M_{\rm gas}/M_\star$[g]	$R_{1/2}/{\rm kpc}$[h]	$N_\star(R_{1/2})/10^5$[i]
A	12.2	4400	0.84		29.3	0.000	1.7	4.64
B	6.7	2500	0.77		10.1	0.007	1.2	1.66
C	2.6	900	0.63		9.5	0.006	3.2	1.62
D	6.7	2400	0.74		13.4	0.001	1.0	1.92
E	3.3	1200	0.48		10.2	0.000	1.2	1.65
F	7.9	2800	0.79		14.5	0.023	0.8	1.89
G	1.2	500	0.81		3.3	0.067	0.7	0.47
H	3.3	1200	0.74		8.0	0.017	1.5	1.35
I	3.3	1200	0.58		8.7	0.057	1.4	1.36
J	2.2	800	0.62		6.2	0.088	1.2	0.89
K	1.1	400	0.59		4.9	0.182	1.4	0.84
AB → A′	18.1	6700	0.67	2257				
H I → H′	6.6	2400	0.62	137	12.5	0.000	2.1	2.09
CD → C′	9.6	3600	0.53	431				
C′E → C″	13.0	4800	0.70	492				
FG → F′	9.3	3400	0.56	511				
C″F′ → C‴	23.1	8500	0.69	537	52.4	0.000	2.5	8.02
JK → J′	5.3	2000	0.64	195	10.9	0.011	1.3	1.61

Notes.
[a] Component labels → remnant label for merger remnants.
[b] SMBH mass.
[c] SMBH to stellar particle mass ratio.
[d] SMBH dimensionless spin parameter.
[e] Merger recoil kick velocity.
[f] Stellar mass within $r < 15$ kpc.
[g] Gas fraction within $r < 15$ kpc.
[h] Projected stellar half-mass–radius.
[i] Number of stellar particles within $R_{1/2}$.

emission. The evolution of the PN-corrected orbital parameters (Memmesheimer et al. 2004; Mannerkoski et al. 2019) of the binaries is shown in Figure 3, and the properties of the merger remnants are listed in Table 1.

Most of the SMBH binaries form at moderately high eccentricities of $e = 0.6$–0.95, with limited eccentricity evolution during the hardening process. These high eccentricities result in relatively short binary lifetimes of ∼200–500 Myr. However, the FG-binary is an exception to this general trend, with a very high peak eccentricity of $e = 0.998$ resulting in an extremely rapid GW-driven merger in just a few tens of megayears. The eccentricity growth occurs when the binary semimajor axis is still above 10 pc, and the mass ratio of the binary is also relatively large (∼7:1), which suggests that resonant dynamical friction (Rauch & Tremaine 1996) might be at work in addition to the eccentricity growth caused by simple stellar scattering (Quinlan 1996). Another exception to the trend of moderately high eccentricities is the low-eccentricity ($e \approx 0.35$) JK-binary, which forms after a nearly circular orbit galaxy merger and takes almost a gigayear to merge. The host galaxies gJ and gK are also gas-rich, leading to significant gas accretion onto the SMBHs during the simulation; however, this accretion does not markedly affect the binary evolution.

Similarly to Mannerkoski et al. (2021), a SMBH triplet also occurs in this simulation (CD-E in Figure 3). After being temporarily ejected to a wider orbit through strong gravitational interactions with the CD-binary, SMBH E settles into a hierarchical triplet configuration around the inner binary. However, contrary to our previous study, the outer orbital period is in this case shorter than the relativistic precession period of the inner binary. This results in von Zeipel–Lidov–Kozai type oscillations (Lidov 1962) that eventually excite the CD-binary eccentricity from $e \approx 0.55$ to a high value of $e \approx 0.9$. At the relatively small semimajor axis of $a \approx 0.12$ pc the increased eccentricity is enough to cause a near instant GW-driven merger of the CD-binary.

3.2. SMBH Ejection and $M_\bullet$–$\sigma_\star$ Relation

The SMBH merger remnants typically experience rather modest GW recoil kicks with velocities below $\lesssim 500\ {\rm km\ s^{-1}}$ (Table 1). Such kicks are not strong enough to displace the SMBHs significantly from the centers of their host galaxies, and typically only result in oscillations of ∼200 pc around the center of the galaxy that are dampened by dynamical friction over a timescale of ∼10 Myr. The one exception is A′, which receives a kick of $2257\ {\rm km\ s^{-1}}$. This is above the galactic escape velocity ($v_{\rm esc} \approx 1950\ {\rm km\ s^{-1}}$) and A′ is thus ejected from its host galaxy, receding to a distance of 4.1 Mpc by the end of the simulation. While such large kick velocities are in general rare, we find that for this particular SMBH spin configuration, the probability of a kick above $2000\ {\rm km\ s^{-1}}$ is about 20%.

The ejection of A′ leads to an interesting evolution of its host galaxy gA on the $M_\bullet$–$\sigma_\star$ plane, as shown in Figure 4. This figure also shows the evolution of galaxies gH and gJ, which undergo mergers without SMBH ejections. The results from the simulation are compared with the observed relation by

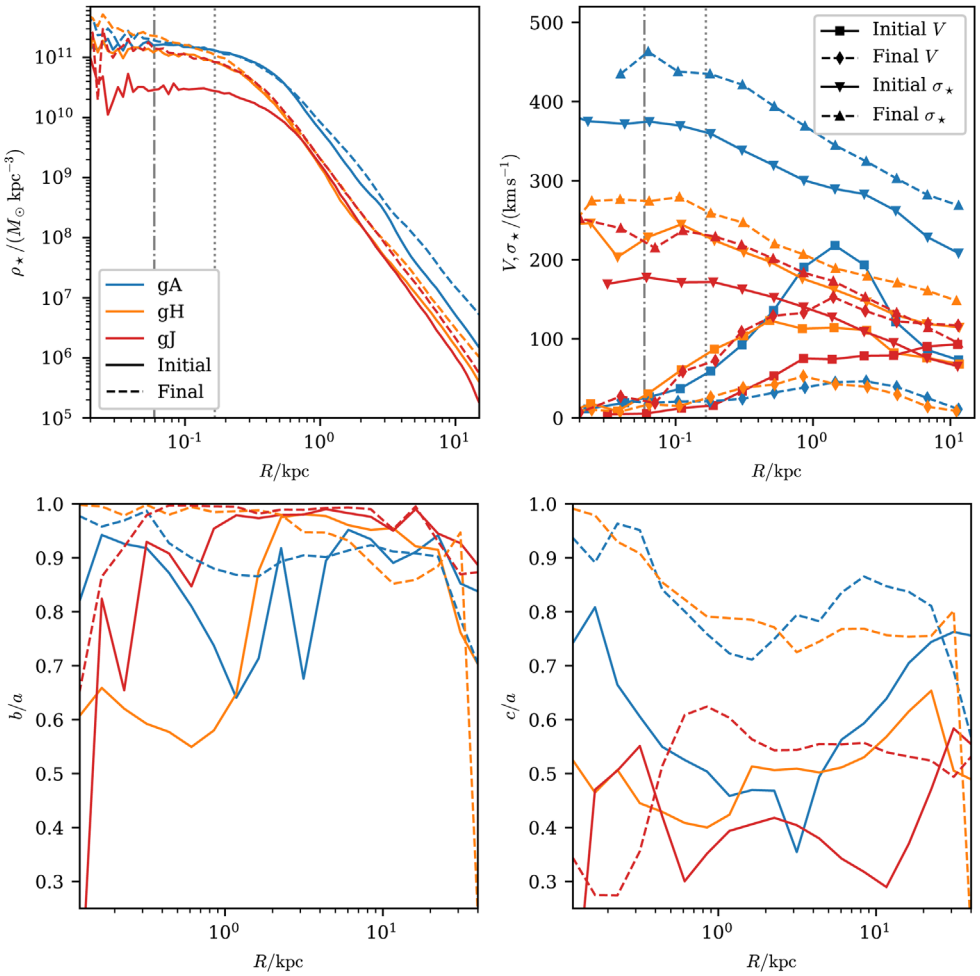

Figure 2. *Top left:* Three-dimensional stellar density profiles in the initial and final states of the KETJU run of the three galaxies (gA, gH, and gJ) remaining in the final output. The vertical dashed–dotted and dotted lines show the $\epsilon_{\rm bar} = 40h^{-1}$ pc softening length and the $2.8\epsilon_{\rm bar}$ softening kernel size used in the initial GADGET-3 run. *Top right:*Projected stellar rotational velocity V and velocity dispersion $\sigma_\star$ profiles of the same galaxies measured along the major rotation axis. Bottom: The axis ratio profiles of the galaxies computed using the S1 method of Zemp et al. (2011).

Kormendy & Ho (2013),

$$\log\left(\frac{M_\bullet}{10^9 M_\odot}\right) = -0.51 + 4.38\log\left(\frac{\sigma_\star}{200\ \mathrm{km\ s^{-1}}}\right), \quad (1)$$

which has an intrinsic scatter of $\epsilon = 0.29$ in $\log M_\bullet$.

Initially gA lies within the range expected from the observed relation, but after A′ is ejected and C enters the galaxy, it becomes significantly offset from the relation at a cosmic time of $t = 7.5$ Gyr. As galaxies gD and gE merge with gA, they bring in their central SMBHs, resulting in a partial recovery of the expected BH mass, with gA moving toward the observed relation. By the end of the simulation the offset falls within the 90% region of the intrinsic scatter of the relation. However, had A′ not been ejected, the galaxy and its SMBH would lie even closer to the expected relation, as is shown in Figure 4 by the open circle corresponding to a shift by the ejected SMBH mass. In contrast, galaxies gH and gJ evolve following the observed relation after their respective mergers.

3.3. Detectability of GW Signals with PTAs

We can estimate whether the GW signal from our simulated SMBH binaries would be individually detectable with PTAs by calculating the signal-to-noise ratio (S/N) including the effects of orbital eccentricity using Equation (65) from Huerta et al. (2015). This method is similar to the semi-analytic GW spectrum calculation that was found to work well in Mannerkoski et al. (2019). We use parameter values that resemble values found in currently operating PTAs (e.g., Alam et al. 2021), setting the number of pulsars to $N_p = 40$, the observation cadence to $\Delta t = 0.058$ yr, and the timing noise to $\sigma_{\rm rms} = 200$ ns. For the duration of observations we choose $T_{\rm obs} = 25$ yr, as this increases the detectability of individual systems considerably compared with the current operation time of ∼12 yr.

The evolution of the S/N values before the mergers of the binaries is shown in the left panel of Figure 5. Following Taylor et al. (2016), binaries with S/N above ∼5 might be detectable as resolved sources, meaning that four out of seven of our simulated SMBH binaries would be detectable starting from ∼10 Myr before the merger. The other binaries would likely not be individually detectable, but would produce a significant contribution to the GW background.

Unlike circular binaries, which only emit GWs with a frequency $f = 2f_{\rm orb}$, eccentric binaries emit a signal containing all harmonics $f = nf_{\rm orb}$ of the orbital frequency. This results in the gradual increase and saw-like oscillation of S/N, as different harmonics pass through the fairly sharp region of

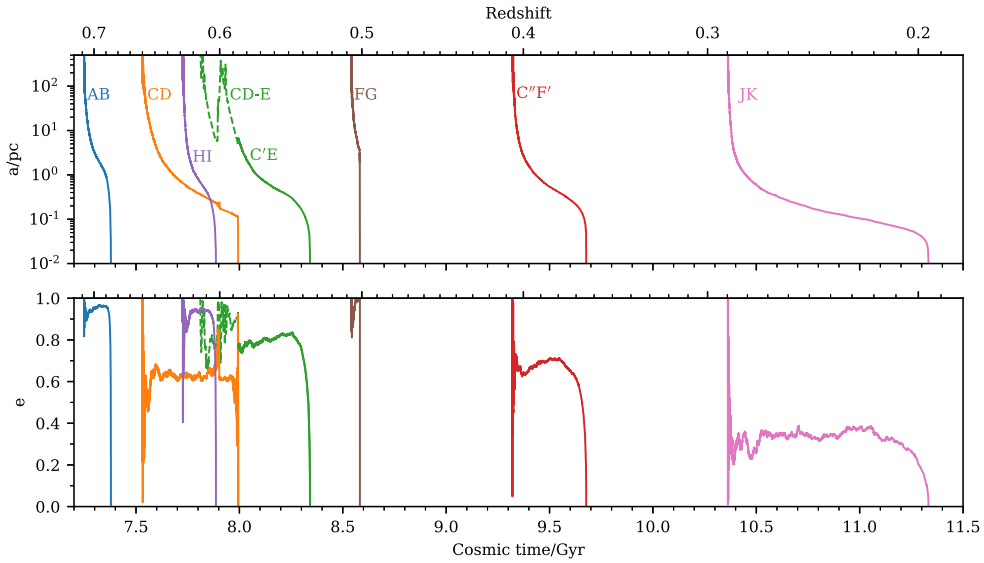

Figure 3. The evolution of the semimajor axis a (*top*) and the eccentricity e (*bottom*) of the simulated SMBH binaries. The dashed line indicates the parameters of the outer orbit in the hierarchical CD-E triplet.

highest sensitivity of the PTA. For the AB and C″F′ binaries the signal is detectable already during a period with significant eccentricity, so that ∼1 Myr prior to the merger the detected GW signal comes from higher harmonics that are not present for a circular binary. In contrast the other binaries become detectable only when the orbits are close to circular and the signal is dominated by the $n = 2$ harmonic.

3.4. Detectability of GW Signals with LISA

The massive SMBH binaries in this study are not prime targets for the planned LISA mission (Amaro-Seoane et al. 2017), as most of their inspiral signal falls below the target frequency sensitivity lower limit of $f = 2 \times 10^{-5}$ Hz. However, the GW signals from the merger and ringdown phases might still be detectable. To test this we calculate the spectra and sky averaged S/N for our SMBH mergers using the BOWIE code (Katz & Larson 2019) and its implementation of the PhenomD waveform (Husa et al. 2016; Khan et al. 2016b).

The right panel of Figure 5 shows the resulting characteristic strain spectra together with the *LISA* sensitivity curve, which is here assumed to extend down to $f = 10^{-5}$ Hz. The S/N calculation yields a high value of 410 for the JK-binary merger, which would therefore be easily detectable. The HI merger with S/N ∼ 55 would likely also be detectable, while CD and FG mergers with S/N ∼ 10 might be marginally detectable if *LISA* reaches the assumed low-frequency sensitivity.

4. Discussion

As the simulation presented here is one of the first cosmological simulations following in detail the small-scale evolution of SMBH binaries, it is of interest to compare the results with earlier isolated collisionless simulations that have shaped the general understanding of SMBH binary evolution. All the SMBH binaries that formed in this simulation were efficiently hardened by stellar interactions without any signs of stalling due to the depletion of the loss cone (Milosavljević & Merritt 2001). This behavior is expected for triaxial galaxies (see bottom panels of Figure 2) that form through mergers (e.g., Berczik et al. 2006; Khan et al. 2013). The eccentric orbits of the binaries are also in general similar to the orbits seen in earlier isolated merger simulations (e.g., Berentzen et al. 2009; Khan et al. 2011; Nasim et al. 2020), which is not too surprising given that merger simulations typically attempt to reproduce the nearly parabolic galaxy merger orbits that are typically found in cosmological simulations (Khochfar & Burkert 2006). The combined effect of eccentric binary orbits and efficient stellar hardening also result in SMBH merger timescales, which are in good agreement with the earlier simulations.

A fundamental difference between the simulations presented here and earlier collisionless merger simulations is the fact that our simulations are run in a full cosmological setting and also include hydrodynamics, star formation, and BH feedback physics. This allows exploring mergers with a more realistic range of parameters compared with the more simplified systems typically used in isolated simulations. However, the general good agreement with earlier isolated merger studies suggests that the various idealizations used in these simulations, such as spherical and isotropic galaxy models, still allow for capturing the general behavior of SMBHs also seen in more realistic galaxies. On the other hand, the lower eccentricity JK-binary was formed in a galaxy merger with a wide inspiraling orbit, and is thus an example of a SMBH merger from a less explored region of the parameter space.

A more detailed understanding of the binary evolution process could potentially be achieved by studying a wide range of SMBH mergers in different environments. This in turn could be used to improve the semi-analytic models used to model the statistics of the cosmologically merging SMBH populations. Although the number of binaries seen here is too small to draw any firm conclusions, the distribution of binary eccentricities seen here does not appear to resemble the simple distributions, e.g., uniform or constant, that have been used in recent studies using such models (e.g., Kelley et al. 2017; Bonetti et al. 2019; Izquierdo-Villalba et al. 2022), which could potentially affect the validity of these results.

The details of the SMBH binary evolution presented here depend on the interactions with the stellar component in the

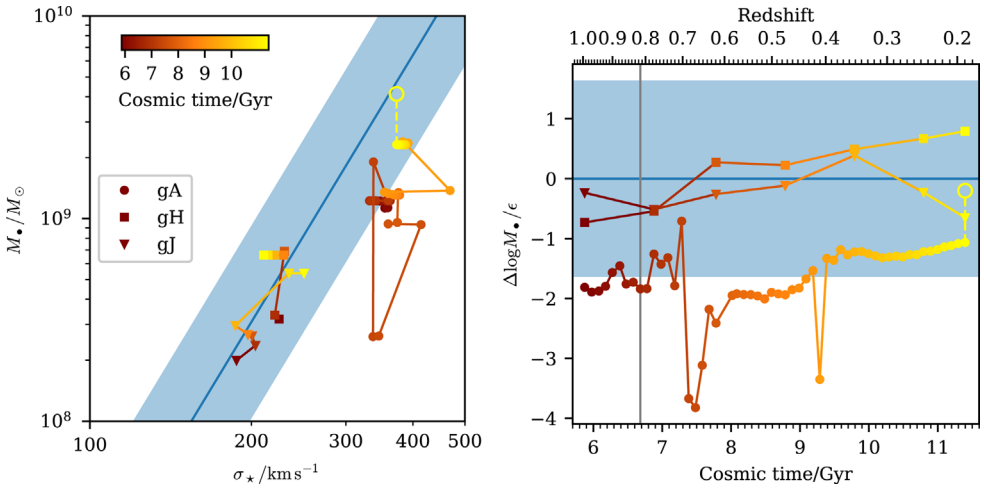

Figure 4. *Left:* The time evolution of the same galaxies (gA, gH, and gJ) as in Figure 2 on the $M_\bullet$–$\sigma_\star$ plane. The line and shaded region show the observed relation (Equation (1)) and the 90% prediction interval corresponding to the intrinsic scatter. The open circle with a dashed line shows where the BH mass would lie without the ejection of A′ from the gA system. *Right:*The time evolution of the difference in mass to the relation in units of the intrinsic scatter ϵ (see also Johansson et al. 2009a). The vertical gray line marks the start of the KETJU run.

center of the galaxies. In cosmological simulations it is challenging to resolve the central regions of galaxies, as the particle masses and gravitational softening lengths have to be sufficiently large for the simulations to be computationally feasible, with this challenge even increasing when higher-accuracy SMBH dynamics, such as in KETJU, are included. These resolution limitations appear to affect our simulation to some extent, as the central galaxy density profiles were seen to flatten, resulting in cores on scales comparable to the softening length. However, the galaxies are still in general well resolved with moderately high numbers of a few hundred thousand stellar particles within their half-mass radii.

The artificially cored density profiles may affect the SMBH binary dynamics by somewhat reducing the number of stellar particles interacting strongly with the binary, which would also reduce the binary hardening rate. The orbits of the particles are also likely to differ from those in a higher-resolution simulation, but how this would affect the dynamics is unclear. The stellar particle counts used to resolve each galaxy, or equivalently the stellar particle masses, may also affect the hardening rate, as isolated *N*-body simulations have found that the binary hardening rates typically converge at $\sim 10^6$ stellar particles or SMBH to stellar particle mass ratios of $\sim$5000. Lower resolutions typically lead to higher hardening rates due to both numerical relaxation effects and Brownian motion of the binary (e.g., Khan et al. 2013; Bortolas et al. 2016). However, the resolution dependence of the hardening rate is rather low in triaxial systems that form after mergers (e.g., Berczik et al. 2006; Khan et al. 2011; Gualandris et al. 2017; Rantala et al. 2017), and the gravitational softening used here in the stellar interactions should also further reduce the resolution dependence caused by relaxation (Gualandris et al. 2017).

The similarity of the binary evolution seen here to that of earlier isolated simulations suggests that the potential issues described above do not compromise our results to any significant degree. The various convergence results found in isolated *N*-body studies may also not generalize to full cosmological simulations, as the structure of the dynamically formed galaxies is significantly different from the idealized models used in the isolated simulations. Further work will also be needed to understand the convergence behavior of the simulations and to produce galaxies with sufficiently resolved central regions. In addition to simply increasing the computational effort in order to decrease the particle masses and softening lengths, the key effort required to achieve this will be developing more physically motivated star formation and BH feedback models, which also account for the dynamically resolved BH binary phase.

The evolution of the $M_\bullet$–$\sigma_\star$ relation due to SMBH recoil kick effects has already been previously studied in isolated merger simulations (Blecha et al. 2011), where the main effect of the kick was to displace the SMBHs from the high-density galactic centers and thus resulting in a reduced gas accretion history. In addition, several studies of the impact of SMBH recoil kicks have been performed using semi-analytic techniques (e.g., Volonteri 2007; Gerosa & Sesana 2015; Izquierdo-Villalba et al. 2020), with some studies finding that very strong superkicks, with velocities in excess of $\gtrsim 5000\,\mathrm{km\,s^{-1}}$, could potentially even kick the SMBHs out of the most massive galaxies, thus producing scatter on the $M_\bullet$–$\sigma_\star$ relation. We showed in this study an explicit example of this mechanism, demonstrating that kicks in excess of $\gtrsim 2000\,\mathrm{km\,s^{-1}}$ are in fact able to eject the SMBH from a massive galaxy in a dynamically resolved cosmological zoom-in simulation and thus affect the evolution of the galaxy on the $M_\bullet$–$\sigma_\star$ plane.

For the GW signals emitted by the binaries we here evaluated only their detectability as resolved sources, because the number of binaries in our study is far too low for evaluating the contribution to the stochastic GW background. Many of the binaries were found to be detectable with PTAs, which is not too surprising given that statistical studies have found massive binaries at $z \sim 0.5$ to be most likely the first individually detected sources (Rosado et al. 2015). However, it is probable that the stochastic background will be detected first (e.g., Kelley et al. 2018), particularly given the moderately high eccentricities of the binaries seen here, which will tend to increase the background signal if they are representative of the typical case (Kelley et al. 2017).

Some of the binaries were also found to be detectable with *LISA*, should they merge during its observation period. This is naturally quite unlikely for any individual system due to the

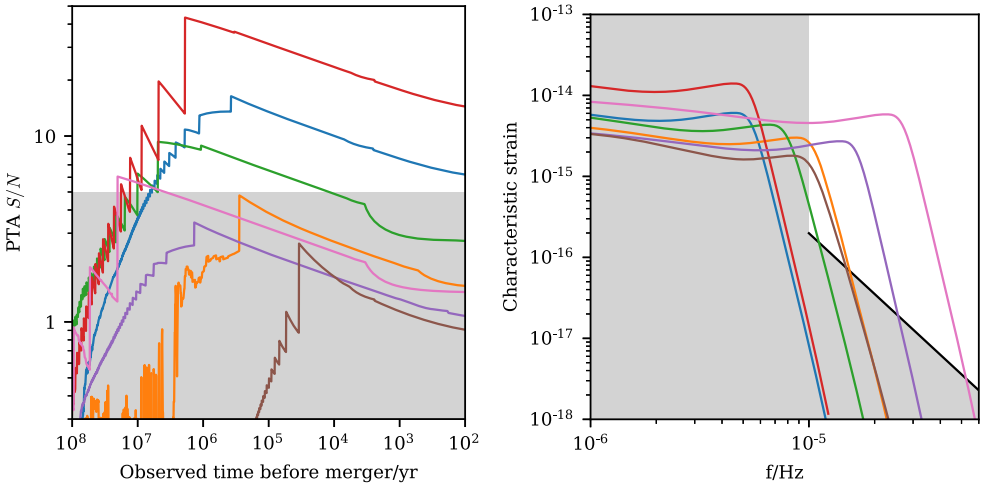

Figure 5. *Left:* The evolution of S/N observed with PTA as a function of time before the merger. The line colors correspond to different binaries as in Figure 3. The shaded region is likely to be unobservable as resolved targets. *Right:* The characteristic strain of the binaries during the final stages of their inspiral and merger. The black line shows the planned *LISA* sensitivity curve. The shaded region is unobservable with the assumed sensitivity.

short planned operation time of only a few years, so this calculation mainly serves as a demonstration that the full orbital evolution of targets relevant for *LISA* can be followed in a cosmological setting using KETJU. Lower-mass SMBH systems, which will be more readily detectable with *LISA*, are typically found in late-type gas-rich galaxies, and thus the simulations require improved accretion and star formation models in order to be modeled properly with KETJU.

5. Conclusions

We have demonstrated that the KETJU code can be used to model the small-scale dynamical evolution of dozens of SMBHs in a complex cosmological environment over long periods of time. Seven SMBH binary systems formed during the simulation, and they were all driven to merger by stellar interactions without any signs of stalling. The detailed dynamical evolution of the SMBH binaries naturally depends on how well the central stellar component is resolved, which is the main limitation of our present study. However, it is encouraging that the results obtained here agree well with simulations of similar systems run in isolation at higher spatial and mass resolutions.

Our simulated SMBH binaries typically formed on quite eccentric orbits, which highlights the need to include the effects of eccentricity for correctly capturing the binary evolution in a majority of the cases. In addition, modeling systems of multiple interacting SMBHs is important for correctly capturing the SMBH merger timescales, as such situations will naturally occur in a cosmological setting. The displacement and ejection of SMBHs by GW recoil kicks will introduce scatter to the observed $M_\bullet$–$\sigma_\star$ relation, but as demonstrated here, it is also possible for a galaxy to recover and evolve back onto the relation under the right circumstances.

Finally, we showed that many of the simulated SMBHs in this study would be potentially detectable with PTAs and *LISA*, if they had existed in the real universe at the observed redshifts. In particular PTAs could potentially detect GW signals from the eccentric orbital phase ∼10 Myr before the merger, whereas *LISA* would be able to detect only the final stages of the SMBH mergers simulated in this study, given their relatively large masses. Simultaneous modeling of the accurate small-scale dynamics and gas dynamics will be particularly important for making GW predictions for *LISA*, as it will be mostly sensitive to SMBHs in the mass range of $M_\bullet \sim 10^5$–$10^7 M_\odot$, which are expected to reside in late-type gas-rich galaxies.

M.M., P.H.J., S.L., and A.R. acknowledge the support by the European Research Council via ERC Consolidator Grant KETJU (no. 818930) and the support of the Academy of Finland grant 339127.

T.N. acknowledges support from the Deutsche Forschungsgemeinschaft (DFG, German Research Foundation) under Germany's Excellence Strategy—EXC-2094-390783311 from the DFG Cluster of Excellence "ORIGINS."

The numerical simulations used computational resources provided by the CSC—IT Center for Science, Finland.

Software: KETJU (Rantala et al. 2017, 2020), GADGET-3 (Springel 2005), NumPy (Harris et al. 2020), SciPy (Virtanen et al. 2020), Matplotlib (Hunter 2007), pygad (Röttgers et al. 2020), MUSIC (Hahn & Abel 2011, 2013), BOWIE (Katz & Larson 2019).

ORCID iDs

Matias Mannerkoski https://orcid.org/0000-0001-5721-9335
Peter H. Johansson https://orcid.org/0000-0001-8741-8263
Antti Rantala https://orcid.org/0000-0001-8789-2571
Thorsten Naab https://orcid.org/0000-0002-7314-2558
Shihong Liao https://orcid.org/0000-0001-7075-6098
Alexander Rawlings https://orcid.org/0000-0003-1807-6321

References

Alam, M. F., Arzoumanian, Z., Baker, P. T., et al. 2021, ApJS, 252, 5
Amaro-Seoane, P., Audley, H., Babak, S., et al. 2017, arXiv:1702.00786
Arzoumanian, Z., Baker, P. T., Blumer, H., et al. 2020, ApJL, 905, L34
Aumer, M., White, S. D. M., Naab, T., & Scannapieco, C. 2013, MNRAS, 434, 3142
Begelman, M. C., Blandford, R. D., & Rees, M. J. 1980, Natur, 287, 307
Berczik, P., Merritt, D., Spurzem, R., & Bischof, H.-P. 2006, ApJL, 642, L21
Berentzen, I., Preto, M., Berczik, P., Merritt, D., & Spurzem, R. 2009, ApJ, 695, 455
Bezanson, R., van der Wel, A., Pacifici, C., et al. 2018, ApJ, 858, 60

Blanchet, L. 2014, LRR, 17, 2
Blecha, L., Cox, T. J., Loeb, A., & Hernquist, L. 2011, MNRAS, 412, 2154
Bonetti, M., Sesana, A., Haardt, F., Barausse, E., & Colpi, M. 2019, MNRAS, 486, 4044
Bortolas, E., Gualandris, A., Dotti, M., Spera, M., & Mapelli, M. 2016, MNRAS, 461, 1023
Campanelli, M., Lousto, C., Zlochower, Y., & Merritt, D. 2007, ApJL, 659, L5
Comerford, J. M., Pooley, D., Barrows, R. S., et al. 2015, ApJ, 806, 219
Eisenreich, M., Naab, T., Choi, E., Ostriker, J. P., & Emsellem, E. 2017, MNRAS, 468, 751
Gerosa, D., & Sesana, A. 2015, MNRAS, 446, 38
Gualandris, A., Read, J. I., Dehnen, W., & Bortolas, E. 2017, MNRAS, 464, 2301
Hahn, O., & Abel, T. 2011, MNRAS, 415, 2101
Hahn, O., & Abel, T. 2013, MUSIC: MUlti-Scale Initial Conditions, Astrophysics Source Code Library, ascl:1311.011
Harris, C. R., Millman, K. J., van der Walt, S. J., et al. 2020, Natur, 585, 357
Hills, J. G., & Fullerton, L. W. 1980, AJ, 85, 1281
Hu, C.-Y., Naab, T., Walch, S., Moster, B. P., & Oser, L. 2014, MNRAS, 443, 1173
Huerta, E. A., McWilliams, S. T., Gair, J. R., & Taylor, S. R. 2015, PhRvD, 92, 063010
Hunter, J. D. 2007, CSE, 9, 90
Husa, S., Khan, S., Hannam, M., et al. 2016, PhRvD, 93, 044006
Izquierdo-Villalba, D., Bonoli, S., Dotti, M., et al. 2020, MNRAS, 495, 4681
Izquierdo-Villalba, D., Sesana, A., Bonoli, S., & Colpi, M. 2022, MNRAS, 509, 3488
Johansson, P. H., Burkert, A., & Naab, T. 2009a, ApJL, 707, L184
Johansson, P. H., Naab, T., & Burkert, A. 2009b, ApJ, 690, 802
Johansson, P. H., Naab, T., & Ostriker, J. P. 2012, ApJ, 754, 115
Katz, M. L., & Larson, S. L. 2019, MNRAS, 483, 3108
Kelley, L. Z., Blecha, L., Hernquist, L., Sesana, A., & Taylor, S. R. 2017, MNRAS, 471, 4508
Kelley, L. Z., Blecha, L., Hernquist, L., Sesana, A., & Taylor, S. R. 2018, MNRAS, 477, 964
Khan, F. M., Fiacconi, D., Mayer, L., Berczik, P., & Just, A. 2016a, ApJ, 828, 73
Khan, F. M., Holley-Bockelmann, K., Berczik, P., & Just, A. 2013, ApJ, 773, 100
Khan, F. M., Just, A., & Merritt, D. 2011, ApJ, 732, 89
Khan, S., Husa, S., Hannam, M., et al. 2016b, PhRvD, 93, 044007
Khochfar, S., & Burkert, A. 2006, A&A, 445, 403
Kormendy, J., & Ho, L. C. 2013, ARA&A, 51, 511
Lidov, M. L. 1962, P&SS, 9, 719
Lim, H., & Rodriguez, C. L. 2020, PhRvD, 102, 064033
Lousto, C. O., Nakano, H., Zlochower, Y., & Campanelli, M. 2010, PhRvD, 81, 084023
Mannerkoski, M., Johansson, P. H., Pihajoki, P., Rantala, A., & Naab, T. 2019, ApJ, 887, 35
Mannerkoski, M., Johansson, P. H., Rantala, A., Naab, T., & Liao, S. 2021, ApJL, 912, L20
Memmesheimer, R.-M., Gopakumar, A., & Schäfer, G. 2004, PhRvD, 70, 104011
Milosavljević, M., & Merritt, D. 2001, ApJ, 563, 34
Naab, T., & Ostriker, J. P. 2017, ARA&A, 55, 59
Nasim, I., Gualandris, A., Read, J., et al. 2020, MNRAS, 497, 739
Nasim, I. T., Gualandris, A., Read, J. I., et al. 2021, MNRAS, 502, 4794
Peters, P. C. 1964, PhRv, 136, 1224
Planck Collaboration, Aghanim, N., Akrami, Y., et al. 2020, A&A, 641, A6
Quinlan, G. D. 1996, NewA, 1, 35
Rantala, A., Johansson, P. H., Naab, T., Thomas, J., & Frigo, M. 2018, ApJ, 864, 113
Rantala, A., Pihajoki, P., Johansson, P. H., et al. 2017, ApJ, 840, 53
Rantala, A., Pihajoki, P., Mannerkoski, M., Johansson, P. H., & Naab, T. 2020, MNRAS, 492, 4131
Rauch, K. P., & Tremaine, S. 1996, NewA, 1, 149
Reynolds, C. S. 2019, NatAs, 3, 41
Rosado, P. A., Sesana, A., & Gair, J. 2015, MNRAS, 451, 2417
Röttgers, B., Naab, T., Cernetic, M., et al. 2020, MNRAS, 496, 152
Scannapieco, C., Tissera, P. B., White, S. D. M., & Springel, V. 2005, MNRAS, 364, 552
Scannapieco, C., Tissera, P. B., White, S. D. M., & Springel, V. 2006, MNRAS, 371, 1125
Sijacki, D., Springel, V., Di Matteo, T., & Hernquist, L. 2007, MNRAS, 380, 877
Springel, V. 2005, MNRAS, 364, 1105
Springel, V., Di Matteo, T., & Hernquist, L. 2005, MNRAS, 361, 776
Taylor, S. R., Huerta, E. A., Gair, J. R., & McWilliams, S. T. 2016, ApJ, 817, 70
Thorne, K. S., & Hartle, J. B. 1985, PhRvD, 31, 1815
Virtanen, P., Gommers, R., Oliphant, T. E., et al. 2020, NatMe, 17, 261
Volonteri, M. 2007, ApJL, 663, L5
Will, C. M. 2014, PhRvD, 89, 044043
Zemp, M., Gnedin, O. Y., Gnedin, N. Y., & Kravtsov, A. V. 2011, ApJS, 197, 30
Zlochower, Y., & Lousto, C. O. 2015, PhRvD, 92, 024022